Electronic Supplementary Material (ESI) for CrystEngComm
This journal is © The Royal Society of Chemistry 2013

Supplementary Information

Structural and Magnetic Investigation of Co^{II}/Mn^{II}-based MIL-53 Analogues with Mixed Ligands of Neutral *N*-oxides and Organic Carboxylates

Yongxin Liu,[a,b] Dan Liu,*[a] Yang Yu,[a] Jin Xu,[a] Xiaohui Han[a,b] and Cheng Wang*[a]

[a] *State Key Laboratory of Rare Earth Resources Utilization, Changchun Institute of Applied Chemistry, Chinese Academy of Sciences, 5625 Renmin Street, Changchun, Jilin 130022 (P.R. China).*

[b] *University of the Chinese Academy of Science, Beijing100049 (P.R. China)*

Corresponding authors. E-mail: cwang@ciac.ac.cn and liudan2007@ciac.ac.cn; Fax: +86-431-85698041; Tel: 86-431-85262770;

Electronic Supplementary Material (ESI) for CrystEngComm
This journal is © The Royal Society of Chemistry 2013

Contents

Fig. S1 Thermal ellipsoid of crystal structures with detailed labels in **1**−**3.**

Fig. S2 The π-π interactions between adjacent pyridine rings in **1**−**3**. The centroid-centroid and planar distances of adjacent μ_2 pyridine rings are 4.06/3.61 Å for **1** (a) and 4.93/(3.53, 3.66) Å for **2** (b). The numbers in parenthesis means there are two values for each of those cases. The closest centroid-centroid distance of pyridine rings is 4.606Å for **3** (c).

Fig. S3 Temperature dependence of the inverse susceptibility for **1**−**5**, as measured in an applied field of 1000 Oe. The solid line represents the best fit to the data.

Fig. S4 Thermal dependence of the ac susceptibilities at different frequencies (a) for **1** and (b) for **2**, respectively.

Fig. S5 The powder magnetization (*M*) vs. field (*H*) hysteresis loops at 2 K for **1** and **2**, respectively.

Fig. S6 The coordination environments of the cobalt ions in **1** (a), **2** (b) and **3** (c).

Fig. S7 Temperature dependence of $\chi_m T$ in **4** and **5** measured at 1000 Oe.

Fig. S8 The powder magnetization (M) vs. field (H) for **4** and **5**.

Fig. S9 Powder and simulated XRD patterns of compounds **1**−**5**.

Fig. S10 TGA curves of **1** and **2** at the heating rate of 10 °C per min.

Fig. S11 IR spectra of the complexes for **1**and **2**.

This journal is © The Royal Society of Chemistry 2013

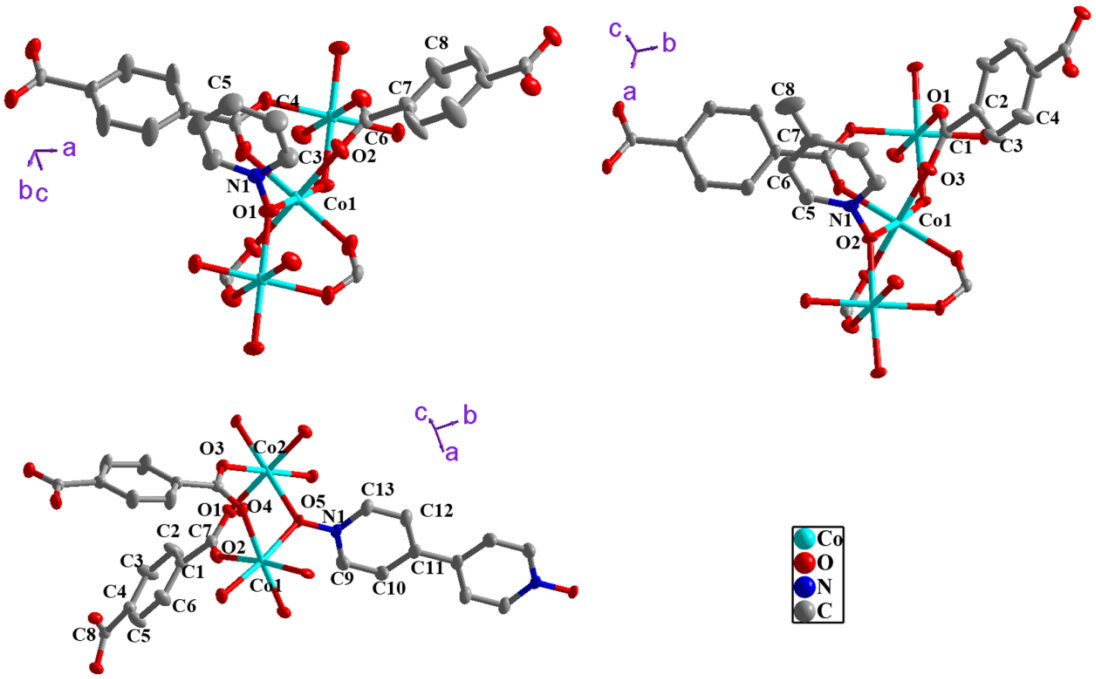

Fig. S1 Thermal ellipsoid of crystal structures with detailed labels in **1**−**3.**

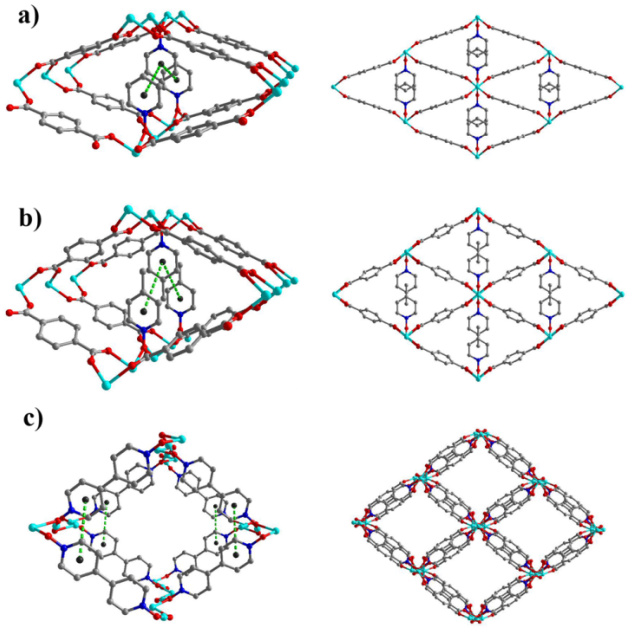

Fig. S2 The π-π interactions between adjacent pyridine rings in **1**−**3**. The centroid-centroid and planar distances of adjacent μ_2 pyridine rings are 4.06/3.61 Å for **1** (a) and 4.93/(3.53, 3.66) Å for **2** (b). The numbers in parenthesis means there are two values for each of those cases. The closest centroid-centroid distance of pyridine rings is 4.606Å for **3** (c).

This journal is © The Royal Society of Chemistry 2013

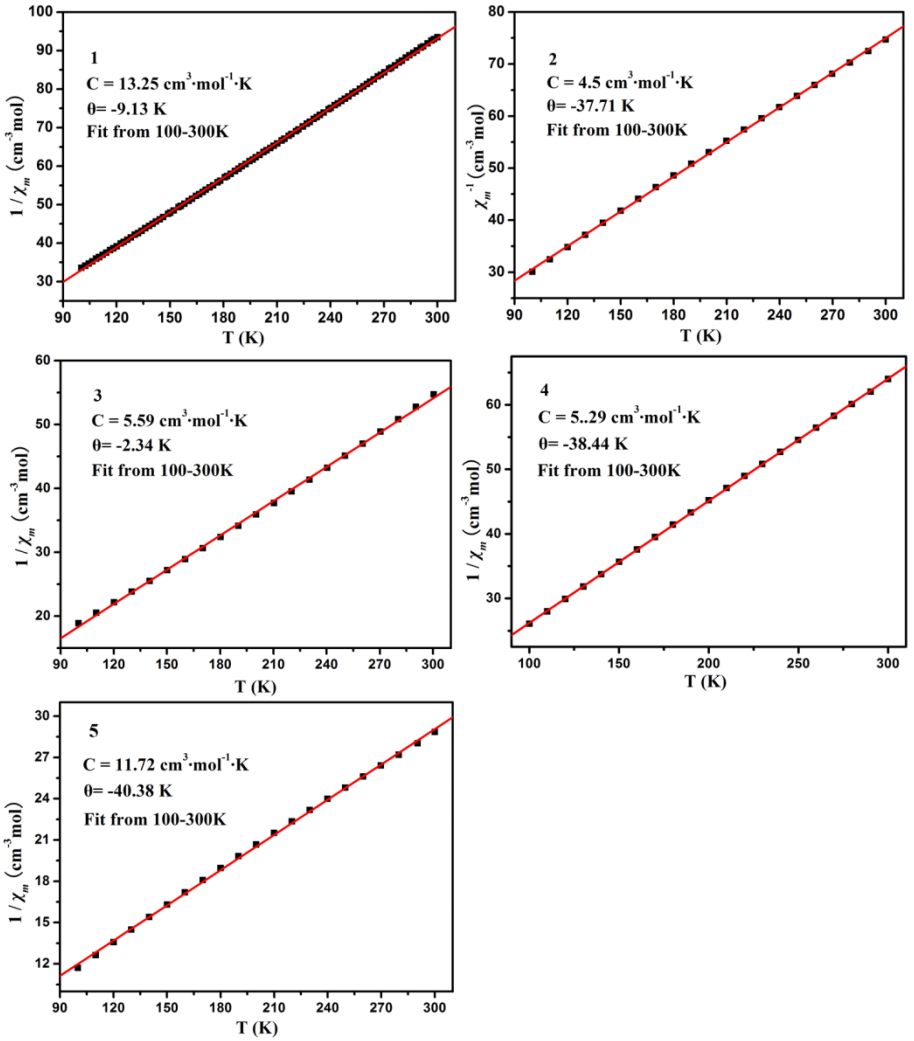

Fig. S3 Temperature dependence of the inverse susceptibility for **1**−**5**, as measured in an applied field of 1000 Oe. The solid line represents the best fit to the data.

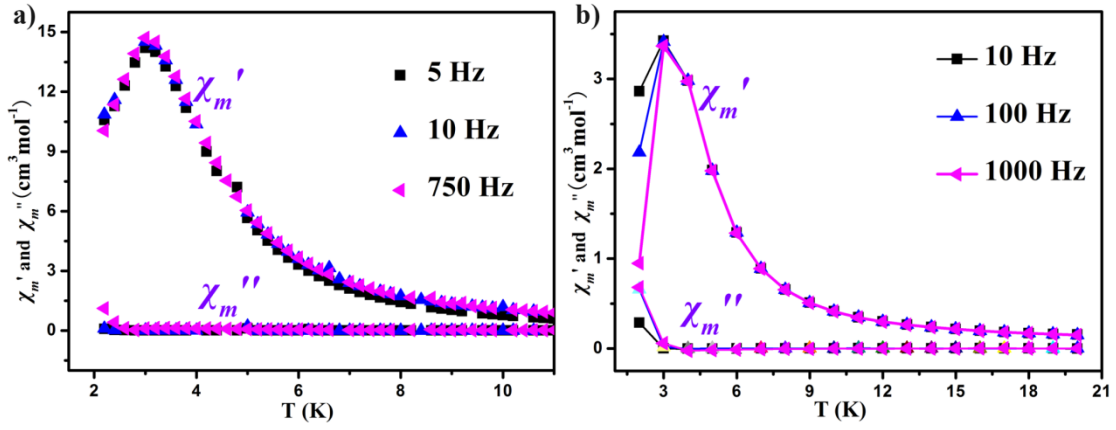

Fig. S4 Thermal dependence of the ac susceptibilities at different frequencies (a) for **1** and (b) for **2**, respectively.

This journal is © The Royal Society of Chemistry 2013

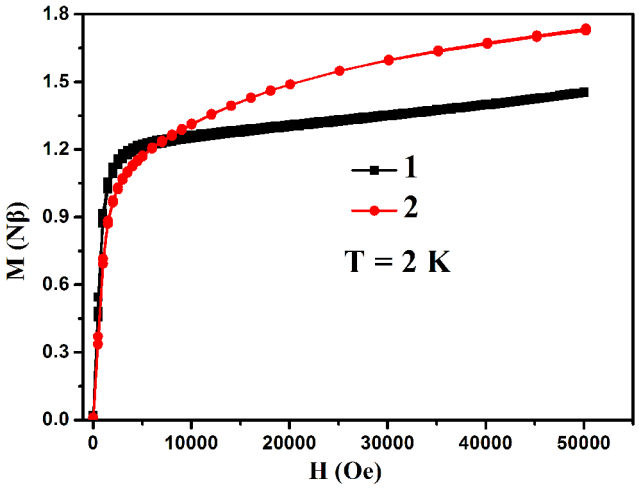

Fig. S5 The powder magnetization (*M*) vs. field (*H*) hysteresis loops at 2 K for **1** and **2**, respectively.

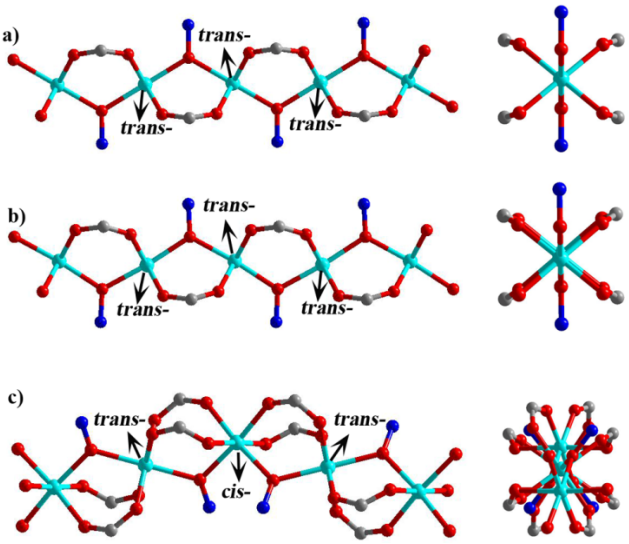

Fig. S6 The coordination environments of the cobalt ions in **1** (a), **2** (b) and **3** (c) (BDC ligands truncated for clarity).

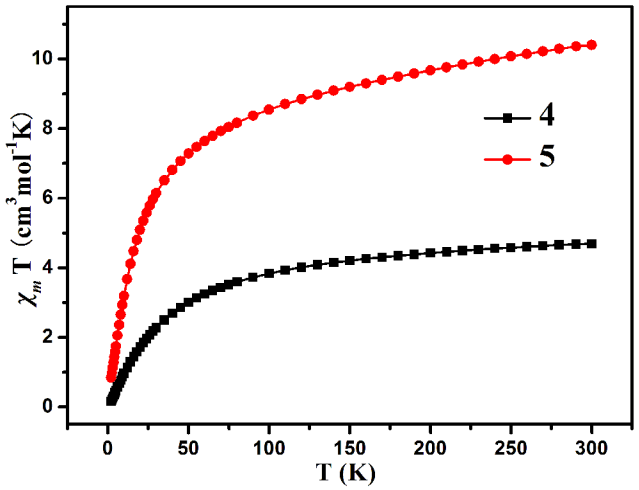

Fig. S7 Temperature dependence of $\chi_m T$ in **4** and **5** measured at 1000 Oe.

This journal is © The Royal Society of Chemistry 2013

Plot of $\chi_m T$ vs. T for **4** is shown in Fig. S7. This plot is the typical for a simple antiferromagnetic system, without any other important features. $\chi_m T$ value (for one Mn(II) ion) is 4.69 $cm^3mol^{-1}K$ for **4** at 300 K, typical value for one Mn(II) ion with g>2.00, and decreases in an unremarkable fashion to 0.16 $cm^3mol^{-1}K$ at 2 K. The Curie–Weiss fits of the inverse magnetic susceptibility above 100 K provide C = 5.29 $cm^3mol^{-1}K$, θ = −38.44 K (Fig. S3). Furthermore, the plot of magnetization (M) vs. field (H) at 2 K (Fig. S8) is clearly indicative of this antiferromagnetic coupling.

As shown in Fig. S7, the $\chi_m T$ value of compound **5** is 10.40 $cm^3mol^{-1}K$ at 300 K, which is much higher than the spin-only to the theoretical spin-only value of 8.75 $cm^3mol^{-1}K$ on the basis of two high-spin octahedral Mn(II) ions (S = 5/2, g = 2.00). Upon further cooling, the $\chi_m T$ value abruptly decreases to a minimum value of 0.85 $cm^3mol^{-1}K$ at 2 K. Magnetic studies show that complex **5** is a typical antiferromagnetic compound with the intrachain antiferromagnetic coupling between adjacent Mn(II) ions, even if a contribution from the spin-orbit coupling of Mn(II) is also present. The susceptibility data above 100 K were well fitted to the Curie-Weiss law, with C = 11.72 $cm^3mol^{-1}K$ and θ = –40.38 K (Fig. S3). The negative value θ indicates an overall antiferromagnetic interaction between the Mn(II) ions. The magnetization versus field measurement (Fig. S8) shows no steps and no hysteresis.

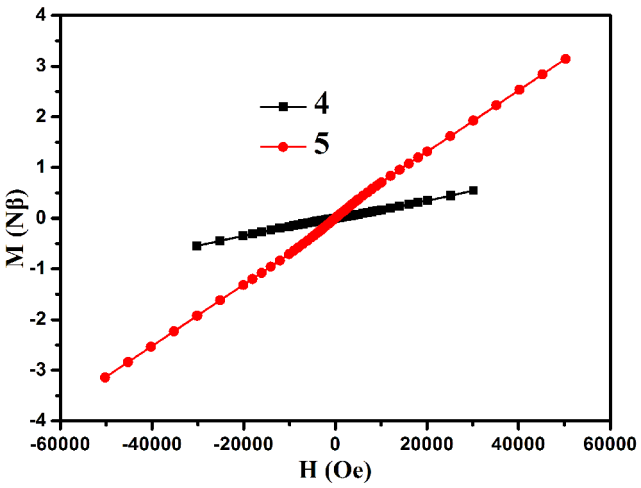

Fig. S8 The powder magnetization (M) vs. field (H) for **4** and **5**.

This journal is © The Royal Society of Chemistry 2013

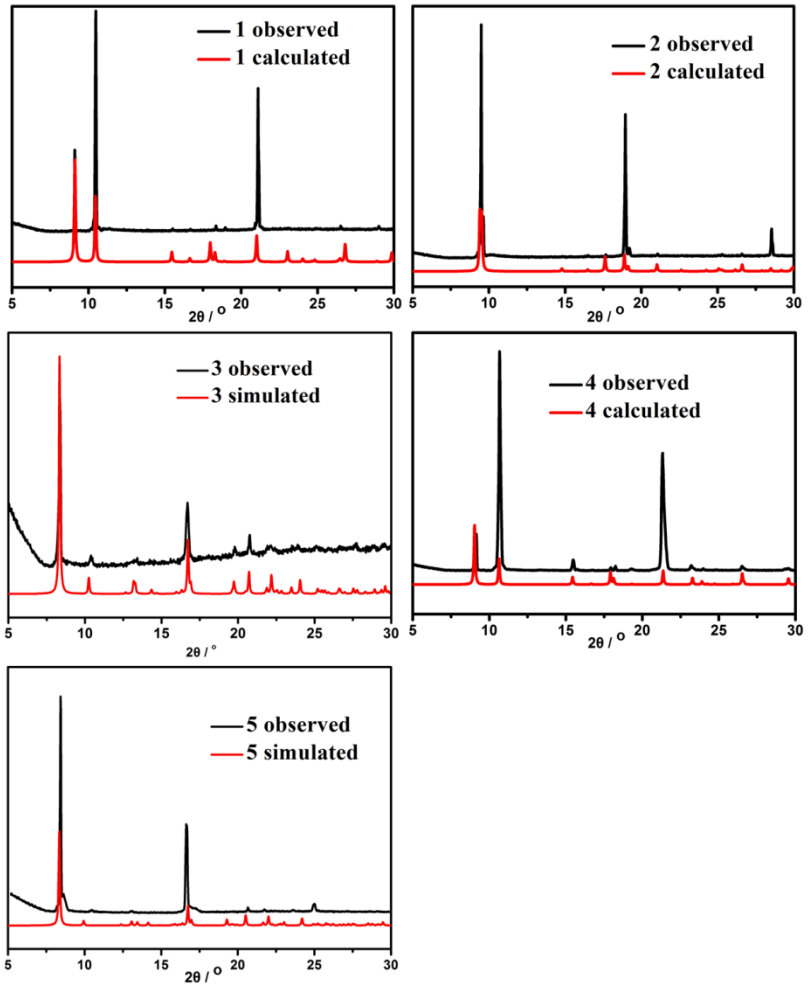

Fig. S9 Powder and simulated XRD patterns of compounds **1**−**5**.

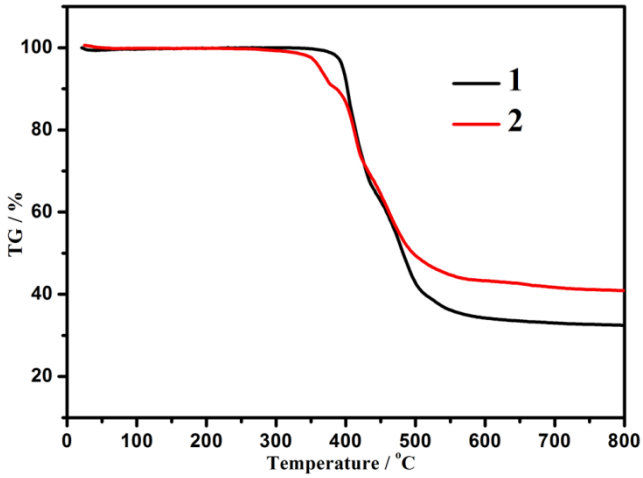

Fig. S10 TGA curves of **1** and **2** at the heating rate of 10 °C per min.

This journal is © The Royal Society of Chemistry 2013

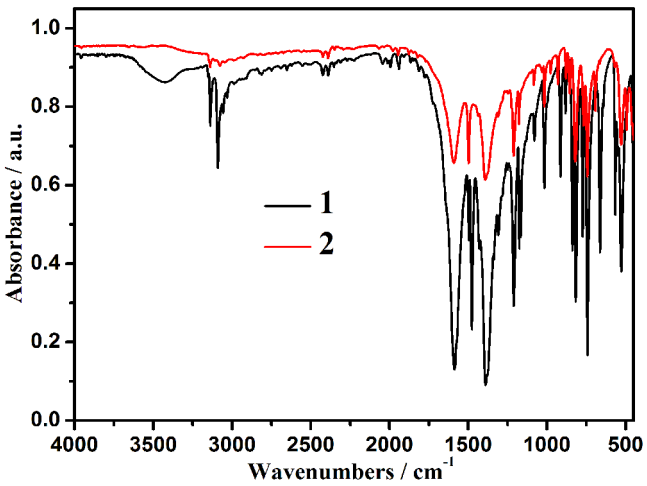

Fig. S11: IR spectra of the complexes for **1**and **2**.